Available *online* at : http://jnte.ft.unand.ac.id/

Jurnal Nasional Teknik Elektro

| ISSN (Print) 2302-2949 | ISSN (Online) 2407-7267 |

Harnessing Sustainable Energy: Portable Pico-Hydro Power Generation Using an Undershoot Water Wheel Turbine in Irrigation Canals

Iftitah Imawati, Galang Ismu Kurniawan, Muhammad Rifan Ghifari, Muhammad Nauval, Fajar Arisandi, Hendra Setiawan, Husein Mubarok

Electrical Engineering Department of Universitas Islam Indonesia, Jalan Kaliurang Km14, Sleman, 55584, Indonesia

ARTICLE INFORMATION

Received: October 9, 2024
Revised: May 22, 2025
Accepted: July 14, 2025
Available online: July 31, 2025

KEYWORDS

pico-hydro, renewable energy, IoT, turbine, irrigation canals

CORRESPONDENCE

Phone: +62 821-3853-2134
E-mail: iftitah.imawati@uii.ac.id

A B S T R A C T

The growing demand for electricity and the environmental impact of fossil fuels have driven the need for alternative, sustainable energy solutions. Hydropower, particularly in irrigation channels, offers a promising option for generating renewable energy. This study focused on developing a small-scale pico-hydro system to generate electricity from water flow in irrigation channels, designed for applications such as street lighting. The research contributes to advancing micro-hydropower technology by integrating an Internet of Things(IoT)-based monitoring system to optimize energy production and simplify performance tracking. The monitoring system enabled real-time tracking of generator output, battery voltage, and load current using a smartphone interface connected via the internet. The study involved laboratory and field testing in some irrigation canals in Yogyakarta, Indonesia. A water wheel turbine from galvanized plates and plastic converts water flow into electrical energy. Field tests confirmed the system's ability to produce stable power. The system reached an overall efficiency of 11.38%. The data transmission delay through Blynk averaged 5.64 seconds, while total power consumption was 2,231 watts. Sensor measurements showed high accuracy, with generator voltage accuracy at 99.33% and load current accuracy at 99.26%. In conclusion, the pico-hydro system can effectively harness irrigation water for small-scale power generation, offering a viable, renewable energy source with efficient remote monitoring capabilities

INTRODUCTION

In Indonesia, irrigation canals are extensively distributed across various regions, representing a largely untapped resource for renewable energy generation. According to data from the Ministry of Public Works and Public Housing (PUPR), Indonesia boasts over 7.2 million hectares of rice fields serviced by irrigation systems, encompassing thousands of kilometers of primary, secondary, and tertiary canals that transport water from its sources to agricultural lands [1] Furthermore, it has been reported that there are approximately 89,000 kilometers of irrigation canals dedicated to watering agricultural fields across the country [2]. Water discharge rates from some irrigation systems in Yogyakarta vary significantly depending on location, season, and climatic conditions, typically ranging from 0.3 to 1 liter per second per hectare of rice field.

During the rainy season, water flow can increase substantially, whereas it tends to decrease in the dry season [3]. The Directorate General of Water Resources indicates that the average water discharge through the primary irrigation systems in some areas of Indonesia is around 10 to 20 cubic meters per second, with larger canals in areas such as Java and Bali often experiencing higher flow rates to meet the greater agricultural water demands [4]. The prevailing irrigation methods in Indonesia primarily utilize the potential energy from flowing water. In addition to serving agricultural needs, these canals present an opportunity to integrate mini pico-hydro power generation systems, harnessing the flowing water's energy to produce electricity without disrupting their primary function of irrigation [5].

The Installation of pico-hydro power generation systems in irrigation canals capitalizes on existing infrastructure, resulting in low-cost renewable energy generation with minimal environmental impact. This has also been reported by [6], [7], [8] [9]. The systems are particularly advantageous for rural areas, providing reliable and sustainable energy access that supports agricultural operations while enhancing energy independence and empowering local communities. By leveraging irrigation water flow, pico-hydro optimizes water resource utilization, diminishes reliance on fossil fuels, and contributes to reducing energy poverty in rural regions.

Several types of turbines used in pico-hydro projects in irrigation channels [6], [10], [11] are Pelton, undershoot water wheels, and screw types. The undershoot turbine was selected for this system not only because of its efficiency at low water flows and minimal head requirements but also because of its portability. Portability is crucial, allowing the system to be easily relocated according to needs and enabling energy use at various points along the channel

https://doi.org/10.25077/jnte.v14n2.1252.2025

without requiring significant permanent installations. This portability is especially beneficial in remote areas where access to energy resources is often limited, as the turbine can be quickly installed and removed, adapting to environmental conditions and fluctuations in water flow without significant disruptions [12]. Additionally, because it does not require complex infrastructure like dams, the system minimizes environmental impact while maintaining the primary function of irrigation channels for agriculture.

The project by [13],[12] also uses a waterwheel turbine for pico-hydro in irrigation canals in Indonesia. Considering these aspects, the undershoot turbine offers a flexible and efficient solution for small-scale hydropower generation, allowing for cost savings in installation and maintenance while facilitating easy monitoring and management through IoT technology. Compared to Pelton and Archimedes turbines, the undershoot turbine is better suited for low head and low flow conditions, making it an ideal choice for irrigation applications where energy generation needs to be adaptable and environmentally friendly [12], [14],[15].

Some pico-hydro systems have maximized efficiency and reliability through real-time performance monitoring using IoT technology [16],[17],[18],[16]. Even slight variations in water flow, turbine positioning, or environmental conditions can significantly impact energy output in low-power systems. This is where the Internet of Things (IoT) becomes essential [19]. The development of this monitoring system utilizes microcontrollers, sensors, wireless communication modules, the Blynk application, and Wi-Fi connectivity to display data on gadgets, such as voltage, current, power, and battery capacity generated by the pico-hydro system.

Additionally, there is a remote light switch feature. With the advancement of technology, villages with internet access can leverage the Internet of Things (IoT) to maximize the performance of pico-hydro power generation. This monitoring system provides benefits for monitoring electricity energy and controlling the power flow to lights generated by the pico-hydro system. In addition to providing real-time readings, it can optimize energy usage. Continuous monitoring allows for damage prevention and extends device lifespan through preventive maintenance. The innovations introduced are expected to enhance the performance of pico-hydro systems and ensure the sustainability of renewable energy in rural areas, ensuring that energy can be monitored and optimized for the common good. This project highlights the potential of similar systems in utilizing existing water infrastructure for renewable energy generation. For instance, remote control of lighting systems can enhance user convenience by eliminating the need for manual switching, as demonstrated in projects utilizing applications such as Blynk to manage lighting via smartphones [20].

A battery stores energy from the generator's conversion in the pico-hydro system. Sensors can be integrated to measure the input and output values to easily determine the battery's capacity, voltage, and current. These readings are processed through a microcontroller program, and the results are transmitted to a web monitoring interface to provide insights into battery capacity as voltage levels [20]. The system consisted of two subsystems, the pico-hydro generation system and the IoT monitoring system.
The integration of pico-hydro power generation systems within Indonesia's extensive irrigation canals presents a remarkable opportunity to harness renewable energy while maintaining the primary agricultural functions of these waterways [18]. Given these opportunities and challenges, this research focused on designing and evaluating a portable pico-hydro power generation system that utilized an undershot waterwheel turbine integrated with an IoT-based monitoring platform.

The system is intended to harness irrigation canal flow for small-scale electricity generation, specifically for rural applications such as street lighting. The integration of IoT enables real-time monitoring, system control, and performance optimization via smartphone, which is crucial for ensuring system reliability and ease of use in remote areas. This research supports Indonesia's renewable energy goals by offering a practical, low-cost, and sustainable solution for decentralized energy access in rural communities.

METHODS

Integration of System

The integration of the entire system is illustrated in Figure 1. There were sensors to measure the DC voltage and current from the pico-hydro system and the battery. After obtaining values for these two parameters, the pico-hydro plant's (PHPP) generated power and the PHPP battery's storage capacity could be determined. A microcontroller was used to process the data collected from the sensors. The processed data was sent to a web server through a wireless communication module for display and storage in a database.

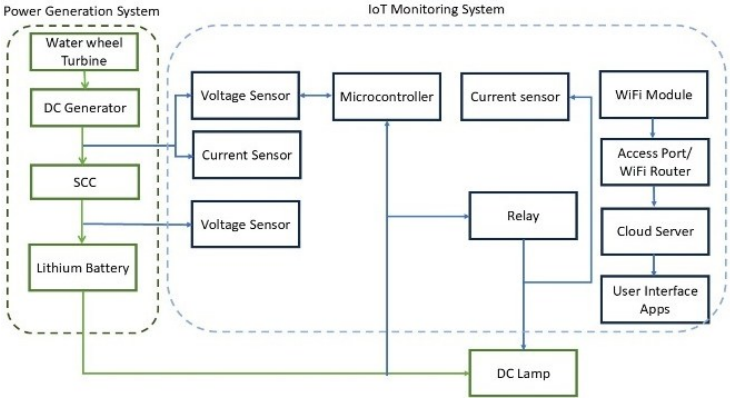

Figure 1 Integration System

The performance monitoring of the pico-hydro system and the battery percentage could be accessed via a smartphone. Furthermore, the output generated by the voltage and current sensors from each measurement, such as the pico-hydro performance and battery percentage, was displayed in real-time, and there was also remote control over the load relay.

Pico-Hydro Power Generation System

The pico hydro power generation sub-system had two major components: a frame, a turbine, and an electrical control panel. The overall system design process was based on the calculation. Pico-hydroelectric power plants harness the difference in elevation and the volume of water flow per second from sources such as irrigation, rivers, or waterfalls. This flow of water turns the turbine shaft to generate mechanical energy. This mechanical energy then powers the generator, producing electricity stored in a battery. Water discharge (Q) refers to the flow rate of liquid passing through a given cross-section over time. It is determined by the velocity (V) and area (A), typically measured in m^3/s, as expressed in Equation (1) [21].

$$Q = V \times A \tag{1}$$

Velocity of water flow and area in this study were measured with Equation (2) and Equation (3), with distance (d), time (t), irrigation width (I), and irrigation depth (D) [21].

$$V = \frac{d}{t} \tag{2}$$

$$A = I \times D \tag{3}$$

Hydroelectric capacity was calculated using the water flow rate. Water flow rate was a key factor in hydroelectric capacity. The parameters were water density (ρ = 0.998 $g/cm3$), gravity, and head height (m). Hydroelectric capacity was calculated using Equation (4) [21].

$$Q = \rho \times g \times Q \times h \tag{4}$$

Turbine rotation speed determined the power output and was affected by the velocity of the water flow (V), the turbine rotation speed measured in rotations per minute (rpm), and was calculated with Equation (5) [22].

$$Tr = \frac{V \times \cos \times \alpha}{2} \tag{5}$$

System efficiency refers to the generator's capability to transform the kinetic energy of flowing water into electrical energy. The efficiency value was determined using Equation 6, which mathematically calculates the efficiency of the electric power generator [21].

$$\eta = \left(\frac{\bar{x} Pg}{Ph}\right) \times 100\% \tag{6}$$

In this study, the system was designed to enable the pico-hydro power plant to be portable, similar to a backpack, and placed on a motorcycle to enhance the portability further. The turbine and frame were hollow and made of galvanised plates, whereas the electrical control panel was made of plastic. The frame had two doors acting as a small reservoir that could increase the water velocity. The turbine specification is shown in Table 1. Turbine specification and the frame and 3D design of the turbine are displayed in Figure 2.

Table 1. Turbine specification

Parameter	Value	Unit
Diameter	30 cm	cm
Number of Blades	16	Piece(s)
Blade Design	70°	Degree
Turbine Weight	2 kg	kg
Turbine Width	15 cm	cm
Material	Galvanism	

The portable pico-hydro system is designed to generate direct current (DC) electricity using a 200-watt DC generator that is mechanically driven by a water wheel turbine. Mechanical energy is transferred from the turbine to the generator through a pulley system with a gear ratio of 1:3. This configuration increases the rotational speed of the generator shaft relative to the turbine, enabling more efficient energy conversion.

Table 2. Power Generation System Specification

Parameter	Value	Unit
Length	50	cm
Width	14	cm
Height	38	cm
Weight	15	kg
Generator Pulley	2	Inch
Turbine Pulley	6	Inch
Generator	200	Watt
SCC	10	A
Battery 3S, 4P	12	Ah
DC Lamp	12	Watt

Once the generator produces electrical energy, it is routed through a solar charge controller. The charge controller plays a critical role in regulating voltage and preventing reverse current flow from the battery back to the generator, thereby protecting the system's components. The regulated current is then used to charge a 12V battery, which serves as the primary energy storage unit. The stored energy can be used to power low-voltage DC loads such as a 12-watt DC lamp or other compatible DC-powered devices. The detailed technical specifications of the power generation system are presented in Table 2, which includes information about the generator capacity, voltage rating, pulley configuration, and control components.

In addition, a visual representation of the entire pico-hydro power generation system is provided in Figure 3, which illustrates the connection and energy flow from the water wheel turbine to the generator, through the charge controller, and finally to the battery and load.

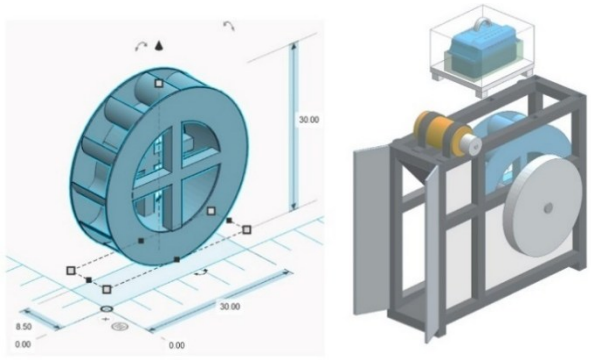

https://doi.org/10.25077/jnte.v14n2.1252.2025

Figure 2. 3D Design of Turbine and System

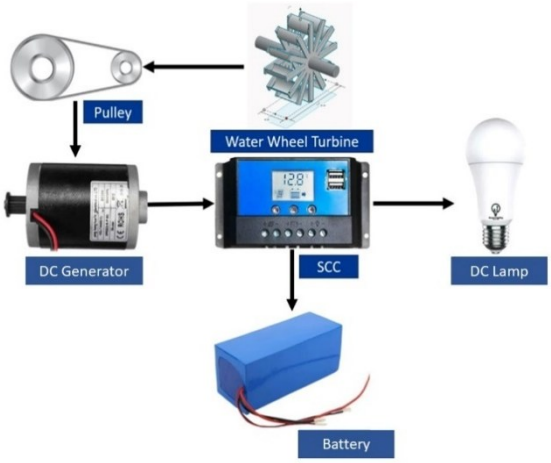

Figure 3 Power generation system

The system was suitable for irrigation and river flow. The system was placed leaning at an angle, as shown in Figure 4. The system was tested in irrigation in Pakembinangun and Hargobinangun, two villages in the Special Region of Yogyakarta. The performance and efficiency of portable pico hydro systems were evaluated using various methods. The field tests assessed the system under three conditions: no load, with a 12W DC lamp load, and complete system (including SCC, battery, and lamp).

These tests aimed to observe how the generator performed without and when connected to a load. Key parameters measured included water flow rate, turbine speed (rpm), generator speed (rpm), generator voltage (volts), generator current (amperes), and power output (watts). Performance assessments were conducted at locations with varying water flow rates to evaluate the device's portability.

Figure 4. An inclined system that operates in village irrigation channels

The system's durability was tested by allowing it to operate continuously for a specified period and then examining its condition. Several methods measured the performance and efficiency of the portable pico-hydro system. For data collection, an electrical box was placed above the water flow to prevent it from being submerged, and the turbine was submerged under a 10 to 15 cm water drop. The positioning during experiments was found to affect turbine rotation significantly. The pulley ratio between the turbine and the generator was 1:3-4, meaning one pulley rotation results in three or four generator rotations. Both laboratory and field experiments used a multimeter for current measurement and a tachometer for the rotational speed of the turbine and generator.

IoT Monitoring System

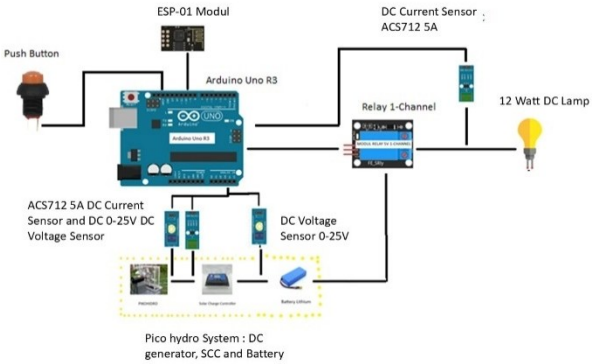

Figure 5 Electronic design for IoT

The IoT monitoring system had two major components: hardware electronics and software with a user interface. The hardware component consisted of Arduino Uno R3 ATmega328P, ESP-01 module, ACS712 current sensor, DC 25V voltage sensor, 1-channel relay module, Blynk platform, push button, and double-layer PCB. The Arduino Uno R3 ATmega328P was chosen for its advanced communication capabilities, making it ideal for developing reliable, responsive, and compact electronic systems.

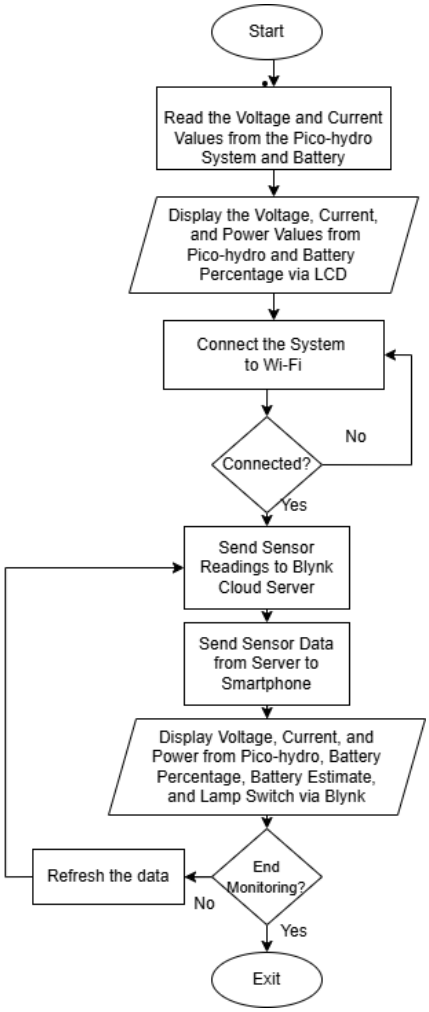

Figure 6 Flowchart Diagram of Real-Time Monitoring and Control in a Portable Pico-Hydro Power Plant using IoT

The 1-channel relay module, operating on an electromagnetic principle, controlled electrical devices such as DC lights, while the Blynk platform facilitated IoT application development, displaying monitoring data and enabling remote control via smartphones. A push button replaced traditional light switches by utilizing the bounce effect to create an electrical signal, and a double-layer PCB organized circuit paths, minimizing the need for extensive wiring. The components were assembled into a unified electronic design as shown in Figure 5. Figure 6 Flowchart Diagram of Real-Time Monitoring and Control in a Portable Pico-Hydro Power Plant using IoTIllustrates the operational steps of the monitoring system integrated into the portable pico-hydro power plant (PHPP).

The PHPP monitoring application has been designed to be accessible via a smartphone using a web-based IoT platform. The application consisted of two main menus. The first menu displayed a switch button and battery percentage, while the second menu showed the pico-hydro output and battery voltage, allowing users to control the lights and view a superchart graph, as illustrated in Figure 7. Application initialization was required to ensure a successful connection to the cloud server. Monitoring data was stored in Blynk's cloud, enabling access at any time.

Figure 7. Application User Interface

Two measurement parameters were utilized in the IoT-based pico-hydro monitoring system: voltage and current. This involved connecting a DC voltage sensor and an ACS712A current sensor to the circuit between the generator and the solar charge controller (SCC), connecting the DC voltage sensor between the SCC and the battery, and connecting the ACS712A current sensor in the circuit between the relay and the load. The measurements were then compared to those obtained using a multimeter to determine the percentage error for each parameter.

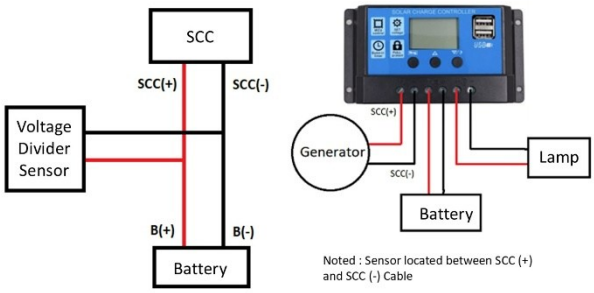

Figure 8 SCC Wiring

Figure 8 Illustrates the voltage and current readings on the generator and SCC paths. As shown in Figure 8, the DC voltage sensor, which had two terminals, was connected to the positive (SCC+) and negative (SCC-) cables. The current sensor's terminals were connected: terminal I1 to cable (G+) and terminal I2 to cable (SCC+). Figure 9 shows the wiring for the sensors.

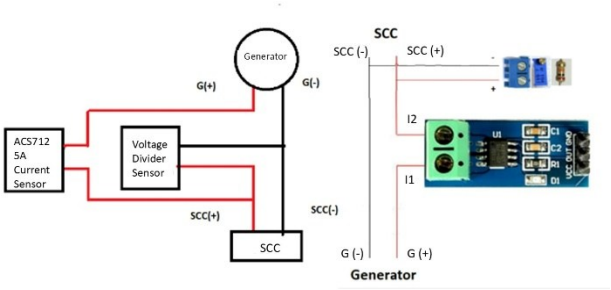

Figure 9 Wiring measurements and placement of voltage and current sensors on the generator

Next, the battery voltage was measured across the SCC and the battery by connecting the DC voltage sensor to the generator's positive (SCC+) and negative (SCC-) terminals. Figure 10 illustrates this setup. To measure the current at the load, the relay connection was established by connecting the (COM) terminal to the (SCC+). The current sensor featured two terminals: terminal I1was connected to the (NO/NC) terminal, while terminal I2 was connected to the (Lamp+). Additional details regarding the sensor wiring can be found in Figure 11.

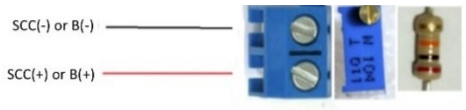

Figure 10 Wiring Voltage Sensor On Battery

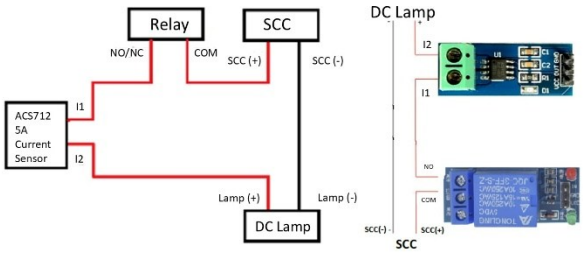

Figure 11 Wiring current measurement and installation of the current sensor, relying on the load

The measurement involved taking sensor readings at 5-second intervals, with three data points being collected for analysis to determine the accuracy and precision of each sensor. The sensor readings were used to calculate the error by comparing them with the multimeter measurements taken simultaneously, using Equation 7. The accuracy was then calculated using Equation 8 [23].

$$Error(\%) = \left|\frac{sensor\ reading\ value - multimeter\ reading\ value}{multimeter\ reading\ value}\right| * 100 \quad (7)$$

https://doi.org/10.25077/jnte.v14n2.1252.2025

$$Accuracy\ (\%) = 100 - Error \quad (8)$$

The average values of the data were calculated using Equation 9, and the standard deviation was determined using Equation 10. Once the average values and standard deviations were calculated, the precision was calculated using Equation 11 [23].

$$Mean(\bar{x}) = \left|\frac{x_1+x_2+\cdots+x_n}{n}\right| \quad (9)$$

where:
Mean(x) : The average of a single data point or the midpoint
$x_1, x_2, .., x_n$: Data n
n : Number of data

$$SD = \sqrt{\frac{\sum_{i=1}^{n}(x_i-\bar{x})^2}{n-1}} \quad (10)$$

where:
SD : Standard Deviation
Mean(x): Average of the data
x_i : Number of single data
n : Number of data

$$Precision\ (\%) = \frac{SD}{\bar{x}} * 100 \quad (11)$$

The testing of battery percentage involved charging a lithium battery of 12V 12AH using a DC voltage sensor, ranging from low to high percentages, and discharging it using a constant current. This method facilitated voltage fluctuation, allowing for comparing voltage measurements obtained from a multimeter. To calculate the battery percentage, Equation 8 was used.

$$Battery\ Percentage = \left(\frac{V_{out}-lower\ limit}{Upper\ limit-lower\ limit}\right) * 100 \quad (8)$$

where :
V_{out} : Voltage read at the battery (sensor/ multimeter) (V)
Lower limit: : Lower voltage limit of the battery (V)
Upper limit : Upper voltage limit of the battery (V)

RESULTS AND DISCUSSION

This section discusses the performance of the portable pico-hydro power system with IoT-based monitoring. Tests were carried out under various conditions to assess the system's power output, voltage stability, and monitoring accuracy. Field testing was done at two irrigation canals in two villages, Pakembinangun and Hargobinangun, to evaluate how the system performed in real conditions. The analysis included no-load and load scenarios by measuring turbine and generator speeds, voltage, current, and power output. Sensor accuracy and IoT data transmission were also examined to ensure reliable monitoring.

Performance of the Pico-Hydro

System No Load Test

Table and Table show the no-load test results from both locations. In Pakembinangun, turbine speeds ranged from 89 to 115 rpm, producing 280 to 457 rpm generator speeds, with voltages between 9.8 V and 13.5 V. The highest voltage was recorded at the fastest generator speed. In Hargobinangun, generator speeds ranged from 307 to 320 rpm, with voltages between 10.2 V and 10.9 V. These results indicate that voltage output increases with rotation speed and is affected by local water flow conditions.

Table 3. Result of No Load Field Test at Pakembinangun

Rotation (rpm)		Voltage (V)
Turbine	**Generator**	
98	423	13.5
109	372	13.2
89	365	13
110	420	13.4
115	457	13.5
107	310	11.2
96	280	10.1
100	285	9.8
110	300	10.2
99	284	10.1

Table 4. Result of No Load Field Test at Hargobinangun

Rotation (rpm)		Voltage (V)
Turbine	**Generator**	
87	312	10.8
91	307	10.2
94	320	10.9
92	311	10.8
97	309	10.4

Load: 12 W DC Lamp

This experiment was carried out by directly connecting the generator to a 12-watt DC lamp as the electrical load. The choice of a 12-watt lamp was based on its power rating, which closely matches the estimated field water power of approximately 14.7 watts. The results of the testing are presented in Table 5 and Table 6.

Table 5. Result of 12-Watt Lamp Test at Pakembinangun

Rotation (rpm)		Power (W)
Turbine	**Generator**	
95	352	1.672
87	300	1.479
93	311	1.584
83	312	1.584
85	369	1.672
97	270	1.215
96	270	1.23
102	278	1.328
100	272	1.312
104	271	1.23

During the testing phase, the lamp operated brightly and stably. The highest lamp output was recorded during the test conducted on July 3 in Pakembinangun. At this location, with an average flow rate of 0.015 m^3/s, the turbine achieved an average rotational speed of 290 rpm, resulting in an average power output of 1.3 watts.

Table 6. Result of 12-Watt Lamp Test at Hargobinangun

Rotation (rpm)		Power (W)
Turbine	Generator	
84	261	1.2
85	263	1.2
88	270	1.215
87	268	1.215
88	270	1.215

Load: Full System (including SCC, battery, and lamp)

The overall system experiment involved the integration of four main components: a generator, a solar charge controller, a battery, and an electrical load. The solar charge controller was equipped with a built-in protection mechanism that restricted the incoming voltage to a maximum of 12.2 V. In this configuration, the generator operated to charge the battery directly. This setup aimed to evaluate the performance of the system under realistic conditions, using actual water flow as the mechanical input source.

Table 7. Result of Full System Test at Pakembinangun

Rotation (rpm)		Power (W)
Turbine	Generator	
98	356	0.732
100	358	0.732
98	350	0.488
98	353	0.488
102	354	0.61
110	315	0.11
121	340	0.46
112	317	0.111
116	322	0.224
119	325	0.23

Field testing was conducted in two locations: Pakembinangun and Hargobinangun. In Pakembinangun, with a stable water flow rate of 0.015 m^3/s, the system demonstrated generator rotational speeds ranging from 315 rpm to 358 rpm. The corresponding electrical power output ranged between 0.11 watts and 0.732 watts, depending on the generator speed and turbine efficiency. These results are detailed in Table 7, which shows that the highest power output of 0.732 W occurred at a generator rotation speed of 356–358 rpm, indicating that the system performs optimally when the turbine reaches around 100 rpm.

Meanwhile, Table 8 presents the test results from Hargobinangun, where the same system was operated under a similar flow rate of 0.015 m^3/s. At this site, generator rotational speeds were slightly lower, ranging from 304 rpm to 315 rpm. Despite the slightly lower mechanical input, the generator was able to produce a higher average electrical output, with power readings between 1.122 W and 1.236 W. The most consistent power generation occurred around a generator speed of 308–312 rpm. These findings suggest that the turbine-generator system in Hargobinangun may have been more efficiently aligned or benefited from reduced mechanical losses, possibly due to site-specific conditions.

Table 8. Result of Full System Test at Hargobinangun

Rotation (rpm)		Power (W)
Turbine	Generator	
88	312	1.236
82	305	1.222
86	308	1.236
91	315	1.224
83	304	1.122

Accuracy and Precision of the System

The testing was conducted with the monitoring prototype for the portable pico-hydro system from the pico-hydro provider, and the system utilizes several components, including a 200W-rated DC generator, a solar charge controller (SCC), a 12V 12AH battery with varying RPM, and a 12-watt light bulb. For each connection path, measurements of generator voltage and current flowing to the SCC, battery voltage, and current flowing to the load through the relay control were taken. The results from testing with different RPMs provide various readings of voltage and current, as detailed in Table 9 and 10.

Table 9. Results of Voltage Reading from RPM Variations

RPM	Multimeter (Volt)	Sensor (Volt)	*Error* (%)	Accuracy (%)
	3.14	3.08	1.91	98.09
100	3.04	2.98	1.97	98.03
	3.1	3.08	0.65	99.35
	6.23	6.23	0.00	100.00
150	6.21	6.18	0.48	99.52
	6.26	6.21	0.80	99.20
	7.64	7.65	0.13	99.87
200	7.67	7.8	1.69	98.31
	7.63	7.65	0.26	99.74
	8.54	8.63	1.05	98.95
250	8.57	8.68	1.28	98.72
	8.6	8.7	1.16	98.84
	8.71	8.72	0.11	99.89
300	8.74	8.75	0.11	99.89
	8.83	8.77	0.68	99.32
	11.9	11.9	0.00	100.00
350	11.89	11.9	0.08	99.92
	11.9	11.9	0.00	100.00
	11.9	11.97	0.59	99.41
400	11.9	11.95	0.42	99.58
	11.9	11.95	0.42	99.58
	11.96	12.02	0.50	99.50
450	11.96	12	0.33	99.67
	11.96	12.05	0.75	99.25
	11.98	12.1	1.00	99.00
500	11.99	12.1	0.92	99.08
	11.98	12.07	0.75	99.25
Mean	-	-	0.67	99.33

https://doi.org/10.25077/jnte.v14n2.1252.2025

The first phase of testing involved collecting data on voltage readings at various RPMs with the generator connected to a solar charge controller (SCC) and a 12V battery, but without any load. The results are shown in Table 9. At the lowest tested RPM (100), the multimeter recorded voltages between 3.04 V and 3.14 V, while the sensor reported values slightly lower, resulting in error rates ranging from 0.65% to 1.97%. Similar trends continued at 150 RPM, where the error ranged from 0% to 0.80%. As the RPM increased, both the sensor and multimeter readings became more consistent. For instance, at 300 RPM, the voltage values from both sources showed a near match, with a minimal error of 0.11% on average. At higher RPMs—350, 400, 450, and 500—the sensor still tracked the multimeter closely, though slight increases in error were observed at 500 RPM, reaching up to 1.00%. Overall, the average error across all RPM levels was calculated to be 0.67%, with a corresponding accuracy of 99.33%, which demonstrates that the voltage sensor operated reliably and within the acceptable tolerance threshold of less than 10%.

Table 10 Current Readings from RPM Variations

RPM	**Multimeter (Ampere)**	**Sensor (Ampere)**	***Error* (%)**	**Accuracy (%)**
	0.5	0.36	28	72
350	0.52	0.39	25	75
	0.5	0.36	28	72
	0.159	0.153	3.77	96.23
400	0.159	0.153	3.77	96.23
	0.159	0.152	4.4	95.6
	0.252	0.223	11.51	88.49
450	0.249	0.231	7.23	92.77
	0.254	0.243	4.33	95.67
	0.359	0.367	2.23	97.77
500	0.361	0.373	3.32	96.68
	0.362	0.388	7.18	92.82
Mean	-	-	10.73	89.27

Complementary to the voltage readings, current measurements were also taken across various RPM levels, as summarized in Table 10. In this test, the measured current represented the charging current delivered to the battery. At RPMs below 300, the multimeter was unable to detect any meaningful current due to the very low values—less than 20 mA—rendering error calculations infeasible. Starting at 350 RPM, measurable currents were detected. The multimeter reported current values around 0.5 A, whereas the sensor output was consistently lower (around 0.36 A), resulting in significant error rates of 25% to 28%. At 400 RPM, the error improved, dropping to between 3.77% and 4.4%. However, at 450 RPM, variability returned, with error rates ranging from 4.33% to 11.51%. At 500 RPM, the error fluctuated between 2.23% and 7.18%. Despite some acceptable values, the overall average error across all readings reached 10.73%, which slightly exceeded the maximum acceptable error of 10%. This suggests that the current sensor, particularly in the generator-side configuration, was less accurate and may require recalibration, filtering, or replacement to ensure compliance with measurement standards [31] .

To thoroughly evaluate the performance of the voltage sensor, additional testing was conducted during the battery charging process, utilizing a 5V 1A adapter connected to an SCC via a specialized charging module. The results of this testing are presented in Table 11, which details the voltage readings collected over time, specifically from 19:00 to 22:40. Throughout this period, the voltage demonstrated a consistent and gradual increase, progressing from 10.69 V to 12.07 V.

A comparative analysis of the voltage sensor readings against those from a multimeter indicated only minor discrepancies, with error percentages ranging from 0.37% to 4.47%. The most significant deviation from the multimeter measurements was observed early in the charging cycle. This initial inconsistency may be attributed to various factors, including potential issues with solder joints, relay performance, and the calibration of the monitoring program.

Table 11. Battery Voltage Readings

Time	**Multimeter Voltage (Volt)**	**Sensor (Volt)**	***Error* (%)**	**Accuracy (%)**
	10.69	10.73	0.37	99.6
	10.75	11.23	4.47	95.5
	11.1	11.29	1.71	98.3
	11.15	11.34	1.70	98.3
	11.18	11.39	1.88	98.1
19.00-22.40	11.23	11.44	1.87	98.1
	11.28	11.49	1.86	98.1
	11.42	11.61	1.66	98.3
	11.88	11.98	0.84	99.2
	11.91	12.05	1.18	98.8
	11.99	12.07	0.67	99.3
	12.02	12.07	0.42	99.6
Mean	-	**11.56**	**1.55**	**98.45**
SD	-	**0.399**	-	-
Precision **(%)**	-	**3.45**	-	-

Figure 12 visually depicts this trend, illustrating how the sensor's readings aligned more closely with the multimeter over time, indicating improved accuracy with continued monitoring. The overall average error calculated for this evaluation was 1.55%, which remains well within the acceptable tolerance limit of less than 10%.

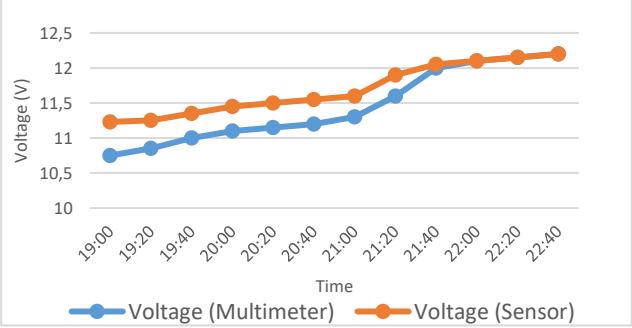

Figure 12 Comparison of Battery Voltage

To complement the voltage magnitude comparison, the sensor's ability to estimate battery percentage was also evaluated. Table 12 compares the battery percentage estimations derived from multimeter voltage data and those reported directly by the sensor. The data show that while the values are generally aligned, discrepancies up to 10% were recorded, particularly early in the test. For example, at 22:00, the multimeter-based percentage was 56%, while the sensor reported 66%, a 10% difference. However, most of the percentage differences stabilized around 1% to 5% as charging progressed. The average battery percentage difference was calculated at 4.6%, indicating reasonable accuracy in estimating state of charge (SoC), though some refinements to the estimation algorithm could enhance reliability.

Table 12 Results of Battery Voltage Percentage Reading

Time	Multimeter Percentage Calculation (%)	Sensor Percentage Calculation (%)	Battery Percentage Difference (%)
22.00-22.20	54	55	1
	56	66	10
	63	68	5
	64	69	5
	65	70	5
	66	71	5
	67	72	5
	70	75	5
	81	83	2
	81	84	3
	83	84	1
	84	85	1
Average Battery Percentage Difference (%)			4.6

A detailed test was performed to evaluate the performance of the current sensor under load conditions, specifically focusing on its capability to power a 12-watt DC lamp through the Smart Control Circuit (SCC). In this experimental configuration, a 5V 4A charging adapter was utilized to provide a stable power supply to the SCC, while a relay was employed to effectively manage the lamp circuit.

The current sensor was responsible for measuring the load current traversing the relay, which provided essential data regarding the system's performance. Table 13 presents the current readings obtained from both the sensor and a multimeter, illustrating their comparative results. As depicted in Figure 13, both the sensor and multimeter readings demonstrated a closely aligned trend throughout the test period.

However, minor deviations were observed at particular points, which can be attributed to real-time fluctuations in the electrical supply or inherent sensor noise. Notably, the average error between the measurements from the two systems was only 0.74%, remaining well within the acceptable 10% tolerance threshold. This outcome confirms that the current sensor exhibited reliable performance under load conditions.

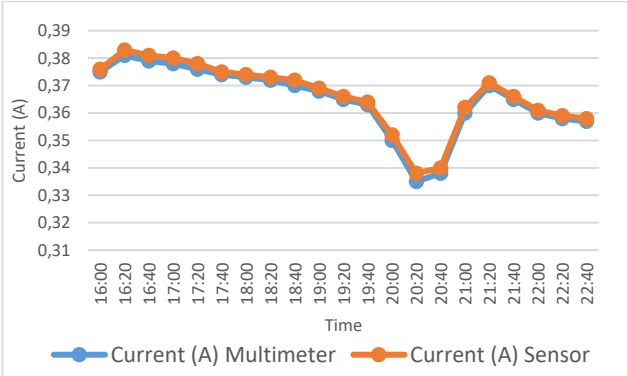

Figure 13 Comparison of 12-Watt Load Current

Table 13. Reading results for 12-watt lamp load current

No	Multimeter (A)	Sensor (A)	*Error* (%)	Accuracy (%)
1	0.371	0.373	0.54	99.46
2	0.374	0.378	1.07	98.93
3	0.381	0.383	0.52	99.48
4	0.377	0.378	0.27	99.73
5	0.372	0.373	0.27	99.73
6	0.376	0.377	0.27	99.73
7	0.369	0.368	0.27	99.73
8	0.371	0.369	0.54	99.46
9	0.376	0.374	0.53	99.47
10	0.374	0.375	0.27	99.73
11	0.372	0.375	0.81	99.19
12	0.369	0.372	0.81	99.19
13	0.368	0.370	0.54	99.46
14	0.346	0.349	0.87	99.13
15	0.342	0.338	1.17	98.83
16	0.335	0.338	0.90	99.10
17	0.359	0.355	1.11	98.89
18	0.361	0.358	0.83	99.17
19	0.355	0.351	1.13	98.87
20	0.355	0.352	0.85	99.15
21	0.359	0.352	1.95	98.05
Mean	-	**0.363**	**0.74**	**99.26**
SD	-	**0.014**	-	-
Precision (%)	-	**3.78%**	-	-

Analysis of the sensor readings indicated that the overall accuracy exceeded 95%, with precision maintained below 4%. It is important to mention that the current sensor associated with the generator revealed a different performance profile. According to the specifications of the multimeter utilized in this assessment, the precision for DC current readings was reported as ±2%, while for DC voltage readings, it was ±0.5%.

https://doi.org/10.25077/jnte.v14n2.1252.2025

As a point of reference, a standard benchmark for precision, relative standard deviation (RSD), or coefficient of variation (CV) is generally considered to be below 2%. This suggests that while the sensors are functioning effectively and exhibit commendable accuracy, there is potential for enhancement regarding their precision.

Discussion and Previous Studies

The portable pico-hydro system demonstrated stable operational performance across both no-load and load conditions. This outcome aligns with findings from prior research on small-scale hydropower technologies, such as those reported in [7] and [25], which emphasizes the reliability of pico-hydro systems in low-resource settings. Under no-load conditions, the system maintained consistent turbine rotation and voltage output, supporting the suitability of the design for light-duty applications such as LED lighting and low-power sensors. However, as noted by [26], one critical factor that significantly affects system behavior under no-load conditions is the accuracy of water discharge measurement. In the present study, while flow rate was held relatively constant at around 0.015 m^3/s, the absence of high-resolution flow instrumentation limited precise correlation analysis between flow variation and turbine rpm. Integrating real-time flow sensors in future iterations could enable more detailed assessments of turbine behavior under varying hydrological inputs and thus facilitate more refined performance modeling and system optimization.

In addition to hydraulic parameters, mechanical characteristics also played a notable role in system performance. One particularly relevant issue observed during testing was related to the transmission system, specifically the belt drive mechanism connecting the turbine to the generator. During operation, it was noted that the use of a slightly uneven belt caused visible dimming of the connected 12-watt lamp whenever the irregular section passed over the generator pulley. This symptom suggests a momentary drop in generator speed or torque, which translates into unstable power delivery to the load. The observation underscores the importance of proper belt alignment and uniform belt thickness, confirming earlier findings such as those in [17], which demonstrated that even minor imperfections in mechanical coupling systems can result in significant electrical output instability. These findings serve as a reminder that although the system is intended to be low-cost and portable, mechanical quality and maintenance remain key contributors to system reliability and efficiency.

In full system testing—where the generator, solar charge controller (SCC), battery, and lamp were integrated—the system exhibited limitations in charging capability, particularly when operating under concurrent load. As presented in Table 7 and Table 8, the power output in Pakembinangun remained below 0.75 W, and although Hargobinangun showed slightly higher values, the output was still marginal relative to the battery's charging requirements. This finding reveals a trade-off between supplying energy to the load and maintaining adequate current for battery storage, especially in low-flow environments. Unlike laboratory-scale systems that often benefit from controlled flow rates and optimized hydraulic heads, field conditions impose natural constraints that significantly reduce system efficiency. As discussed in [14], enhancing the design of the turbine intake—either by optimizing nozzle geometry or reducing friction losses—could increase the effective water velocity and volumetric flow reaching the turbine, thereby improving rotational speed and energy conversion. Additionally, it was suspected that the series connection between the battery and the lamp may have contributed to voltage drops, resulting in underperformance during charging. This contrasts with the findings in [26], which reported a complete charging cycle over 21 hours using a similar battery configuration, but without simultaneous load. Therefore, isolating the battery from the load during future trials may yield more representative data on pure charging performance.

Despite these limitations, the system demonstrated measurable energy conversion efficiency. Based on a hydraulic power input of approximately 14.7 W and a peak electrical output of 1.672 W, the calculated overall efficiency was 11.38%. Although this value is lower than that reported in highly optimized laboratory-scale pico-hydro systems—such as those employing custom turbines or advanced power electronics [27]—The result remains acceptable within the context of real-world field deployment. The system was intentionally built using accessible, low-cost components and designed to function under low-head, low-flow conditions common in rural settings, which inherently restrict maximum efficiency potential.

From a monitoring perspective, the performance of the voltage and current sensors was highly satisfactory. The voltage sensor achieved an average accuracy of 99.33% when compared with multimeter readings across a wide RPM range (see Table 9), while the current sensor used under load conditions achieved 99.26% accuracy (see Table 13 and Figure 13). Although precision did vary depending on specific conditions—particularly with the generator-side current sensor, which exhibited an error above 10% at certain RPMs—response times and trend consistency were sufficient to support real-time monitoring applications. These results suggest that, with minor refinements to hardware assembly and software calibration, the sensing system is robust enough for integration into IoT-based platforms for continuous monitoring and remote diagnostics.

Taken together, the results of this study highlight both the feasibility and the current limitations of deploying portable pico-hydro systems in rural, off-grid environments. The compact form factor, ease of transport, and relatively stable electrical output make the system particularly suited for decentralized renewable energy initiatives targeting small household or community-scale loads. The integration of real-time sensing and data acquisition also adds value by enabling remote visibility and predictive maintenance. However, in order to fully support battery charging and load operation concurrently, further design improvements are needed. These may include increasing turbine efficiency, decoupling loads during charging, and improving mechanical component quality.

In conclusion, this research provides practical evidence supporting the application of low-cost, sensor-integrated pico-hydro systems in real-world settings. The findings underscore the importance of not only hydraulic and electrical design considerations, but also mechanical reliability and intelligent monitoring. While challenges remain—particularly in achieving

efficient energy storage—the work contributes valuable data and insight to the growing field of decentralized renewable energy solutions, and supports the broader goal of sustainable, accessible electrification for off-grid communities.

CONCLUSIONS

The portable pico-hydro system with IoT-based monitoring successfully generated electricity from irrigation canal flow and powered a DC lamp. At a flow rate of 0.015 m^3/s, the system produced 1.672 W with 11.38% efficiency. Although stable, the generator output was not sufficient for fast charging. The IoT system provided reliable, real-time data with minimal delay and high sensor accuracy. This system is suitable for rural, low-power use, but improvements in energy output and charging efficiency are needed.

REFERENCES

[1] M. Haerul, D. Santoso, S. Tp, M. Si, and S. Sirait, "PENGENALAN IRIGASI PERTANIAN PENERBIT CV.EUREKA MEDIA AKSARA."

[2] Kementerian Pertanian, "Statistik Lahan Pertanian Tahun 2015-2019," *Stat. Lahan Pertan. Tahun 2015-2019*, p. 201, 2020.

[3] P. Daerah, I. Yogyakarta, B. S. Wibowo, F. Nurrochmad, E. Prima, and A. Pratiwi, "Analisis Efisiensi Saluran Irigasi Pada Daerah Irigasi Cokrobedog Dan," no. 2017, pp. 1–6, 2024.

[4] R. Tirtalistyani, M. Murtiningrum, and R. S. Kanwar, "Indonesia Rice Irrigation System: Time for Innovation," *Sustain.*, vol. 14, no. 19, 2022, doi: 10.3390/su141912477.

[5] S. R. Ma'Mun, A. Loch, and M. D. Young, "Sustainable irrigation in Indonesia: A case study of Southeast Sulawesi Province," *Land use policy*, vol. 111, Dec. 2021, doi: 10.1016/j.landusepol.2021.105707.

[6] M. Santoshkumar *et al.*, "Design and Development of Pico Hydro Power System By Irrigation Water," *Int. Res. J. Eng. Technol.*, no. June, 2016.

[7] S. P. Adhau, R. M. Moharil, and P. G. Adhau, "Mini-hydro power generation on existing irrigation projects: Case study of Indian sites," *Renew. Sustain. Energy Rev.*, vol. 16, no. 7, pp. 4785–4795, 2012, doi: 10.1016/j.rser.2012.03.066.

[8] M. Alatas, M. T. Sri Budiastuti, T. Gunawan, and P. Setyono, "The Potential of Micro-hydro Power Cascade in Irrigation Channel of Kalibawang, Indonesia," vol. 11, no. 5, 2021.

[9] T. S. Mogaji, S. T. Fasasi, A. O. Ogundairo, and I. A. Oluwagbemi, "Design and Simulation of a Pico Hydroelectric Turbine System," *Futa J. Eng. Eng. Technol.*, vol. 16, no. 1, pp. 132–139, 2022, doi: 10.51459/futajeet.2022.16.1.418.

[10] A. Asral, "Experimental study of Undershot Type Water Wheels as Picohydro Power Generators in Irrigation Channels," *Proksima*, vol. 1, no. 2, pp. 39–42, 2023, doi: 10.31258/proksima.v1i2.12.

[11] Adlan, S. K. Saptomo, and Prastowo, "Pico hydro turbine building design utilizing irrigation water power: CFD Simulation," in *IOP Conference Series: Earth and Environmental Science*, IOP Publishing Ltd, Oct. 2021. doi: 10.1088/1755-1315/871/1/012038.

[12] E. Quaranta and R. Revelli, "Gravity water wheels as a micro hydropower energy source: A review based on historic data, design methods, efficiencies and modern optimizations," *Renew. Sustain. Energy Rev.*, vol. 97, pp. 414–427, 2018.

[13] Y. Hasyim, A. Asral, and F. Murdiya, "Development of Pico-Hydro Electric Power Plant on Irrigation Canal - Case Study: Menaming Village, Indonesia," *J. Ocean. Mech. Aerosp. -science Eng.*, vol. 67, no. 2, pp. 47–54, Jul. 2023, doi: 10.36842/jomase.v67i2.342.

[14] D. Hamdani and M. L. Edypoerwa, "Study and Design of Picohydro Power Plant for Low-Head and Low-Flow Application," vol. 13, no. 2, pp. 200–214, 2025.

[15] V. Uniyal, A. Karn, and V. P. Singh, "Comparative life cycle assessment of micro water Turbines: Evaluating potential for remote power generation," *Sustain. Energy Technol. Assessments*, vol. 73, no. November 2024, p. 104107, 2025, doi: 10.1016/j.seta.2024.104107.

[16] N. Yuniarti, D. Hariyanto, S. Yatmono, and M. Abdillah, "Design and Development of IoT Based Water Flow Monitoring for Pico Hydro Power Plant," *Int. J. Interact. Mob. Technol.*, vol. 15, no. 7, pp. 69–80, 2021, doi: 10.3991/ijim.v15i07.18425.

[17] F. Hazrina and P. Purwiyanto, "Design of Pico-Hydro Power Plant with Monitoring System Based on Internet of Things," *Andalas J. Electr. Electron. Eng. Technol.*, vol. 2, no. 2, pp. 43–49, Dec. 2022, doi: 10.25077/ajeeet.v2i2.29.

[18] B. N. Fortaleza, R. O. Serfa Juan, and L. S. Karlo Tolentino, "IoT-based Pico-Hydro Power Generation System using Pelton Turbine".

[19] K. K. Patel, S. M. Patel, and P. G. Scholar, "Internet of Things-IOT: Definition, Characteristics, Architecture, Enabling Technologies, Application & Future Challenges," *Int. J. Eng. Sci. Comput.*, vol. 6, no. 5, pp. 1–10, 2016, doi: 10.4010/2016.1482.

[20] P. Arjun, S. Stephenraj, N. Naveen Kumar, and K. Naveen Kumar, "A study on IoT based smart street light systems," *2019 IEEE Int. Conf. Syst. Comput. Autom. Networking, ICSCAN 2019*, vol. 8, no. 07, pp. 7–9, 2019, doi: 10.1109/ICSCAN.2019.8878770.

[21] A. Harvey, "Micro-Hydro Design Manual," *Micro-Hydro Des. Man.*, 1993, doi: 10.3362/9781780445472.

[22] D. Kodirov and O. Tursunov, "Calculation of Water Wheel Design Parameters for Micro Hydroelectric Power Station," *E3S Web Conf.*, vol. 97, no. May, 2019, doi: 10.1051/e3sconf/20199705042.

[23] P. AKNIN *et al.*, "Fundamentals of Instrumentation and Measurement," pp. 1–555, 2016.

[24] A. Agrawal and D. Toshniwal, "Fault Tolerance in IoT: Techniques and Comparative Study," *Asian J. Converg. Technol.*, vol. 7, no. 1, pp. 49–52, 2021, doi: 10.33130/ajct.2021v07i01.011.

[25] E. Eswanto, H. Hasan, and Z. M. Razlan, "An Analysis on Performance of Pico-hydro with Archimedes Screw Model Viewed from Turbine Shaft Angle," *Int. J. Eng. Trans. A Basics*, vol. 36, no. 1, pp. 10–18, 2023, doi: 10.5829/ije.2023.36.01a.02.

[26] Y. Apriani, S. Hidayat, Z. Saleh, W. A. Oktaviani, and I. Mochamad Sofian, "Modeling Design of Picohydro Power Generation System Using Crossflow Turbine," *East Asian J. Multidiscip. Res.*, vol. 3, no. 4, pp. 1501–1512, 2024, doi: 10.55927/eajmr.v3i4.8830.

[27] E. Gallego, A. Rubio-Clemente, J. Pineda, L. Velásquez, and E. Chica, "Experimental analysis on the performance of a pico-hydro Turgo turbine," *J. King Saud Univ. - Eng. Sci.*, vol. 33, no. 4, pp. 266–275, 2021, doi: 10.1016/j.jksues.2020.04.011.

https://doi.org/10.25077/jnte.v14n2.1252.2025

AUTHOR(S) BIOGRAPHY

Iftitah Imawati, S.T., M.Eng
She is an expert in power systems, electric machines, and electric vehicles. She earned her Bachelor's degree (S.T.) and Master's degree (M.Eng.) from Universitas Gadjah Mada, Indonesia. Her research focuses on enhancing the efficiency and sustainability of renewable energies and exploring innovations in electric vehicle technology. She can be contacted via email at iftitah.imawati@uii.ac.id

Galang Ismu Kurniawan
He is an electrical engineering student with a keen interest in power systems and generation systems. He is dedicated to exploring innovative solutions in energy production and management. His academic pursuits aim to enhance the efficiency and sustainability of electrical systems. He can be reached via email at 20524117@students.uii.ac.id

Muhammad Rifan Ghifari
He is an electrical engineering student with a keen interest in power systems and generation systems. He is dedicated to exploring innovative solutions in energy production and management. His academic pursuits aim to enhance the efficiency and sustainability of electrical systems. He can be reached via email at 20524121@students.uii.ac.id

Muhammad Nauval
He is an electrical engineering student with a strong interest in the field of Internet of Things (IoT). His academic endeavors focus on integrating IoT technologies into everyday systems to improve functionality and connectivity. He can be reached via email at 20524182@students.uii.ac.id

Fajar Arisandi
He is an electrical engineering student with a strong interest in the field of Internet of Things (IoT). His academic endeavors focus on integrating IoT technologies into everyday systems to improve functionality and connectivity. He can be reached via email at 20524173@student.uii.ac.id

Dr. Eng. Hendra Setiawan, S.T., M.T.
He is an expert in electronics, FPGAs, signal processing, and the wireless communication physical layer. He holds a Bachelor's degree (S.T.) from Universitas Gadjah Mada, a Master's degree (M.T.) from Institut Teknologi Bandung, and a Doctorate (Dr. Eng.) from Kyushu Institute of Technology, Japan. His research focuses on advancing wireless communication technologies and developing efficient electronic systems. He can be reached via email at **hendra.setiawan@uii.ac.id**

Husein Mubarok S.T., M.Eng
He is an expert in energy audit, energy management, renewable energy, and energy conversion. He earned both his Bachelor's degree (S.T.) and Master's degree (M.Eng.) from Universitas Gadjah Mada, Indonesia. His professional focus revolves around sustainable energy solutions and optimizing energy systems to improve efficiency and reduce environmental impacts. You can reach him via email at **155241305@uii.ac.id**